Proton scattering observables from Skyrme-Hartree-Fock densities

S. Karataglidis,[1, *] K. R. Henninger,[2, †] W. A. Richter,[3, ‡] and K. Amos[4, §]

[1]*Department of Physics, University of Johannesburg,*
P.O. Box 524, Auckland Park, 2006, South Africa
[2]*Department of Physics and Electronics, Rhodes University,*
P.O. Box 94, Grahamstown, 6140, South Africa
[3]*Department of Physics, University of the Western Cape,*
Private Bag X17, Bellville 7530, South Africa
[4]*School of Physics, The University of Melbourne, Victoria 3010, Australia*

(Dated: August 11, 2010)

Abstract

Proton and neutron densities from Skyrme-Hartree-Fock (SHF) calculations are used to generate non-local (g-folding) proton-nucleus optical potentials. They are formed by folding the densities with realistic nucleon-nucleon interactions. The potentials are then used to calculate differential cross sections and spin observables for proton scattering. Good agreement with data has been found, supporting those found previously when using SHF charge densities in analyses of electron scattering data. That agreement was improved by use of (shell model) occupation numbers to constrain the HF iterations. That, in part, is also the case with analyses of proton scattering data. The g-folding method is extended to exotic nuclei by including data for neutron-rich sd-shell nuclei from the inverse kinematics of scattering from hydrogen.

---

[*] stevenka@uj.ac.za

[†] g06h0128@campus.ru.ac.za

[‡] richter@sun.ac.za

[§] amos@unimelb.edu.au

1

I.   INTRODUCTION

Nucleon-nucleus (NA) scattering probes the matter density of the nucleus, and of particular interest are the separate density distributions of protons and neutrons. The differences between the two densities become increasingly important as one moves away from the valley of stability towards the drip lines, with the emergence of structures such as halos and skins. Those structures influence NA scattering, whence the problem becomes one of how to extract such information from measurement. For detailed information on the matter (proton and/or neutron) density of the target nucleus one requires a microscopic description of the interaction between the projectile and the target, necessitating also a microscopic (nucleon-based) description of the nucleus.

For radioactive nuclei, experiments have been done in inverse kinematics with a beam of nuclei incident on a hydrogen target. Thus the calculation of differential cross sections and spin observables requires some microscopic model structure for the exotic nucleus, which determines the ground-state densities. The adequacy of the model assumed, for stable nuclei, can be checked against information obtained from the elastic scattering of electrons. The electron scattering form factors are measures of the charge and current densities of the nucleus. While electron scattering data for exotic nuclei are not presently available, the SCRIT experiment [1] and the electron-ion collider ELISe at FAIR [2] will measure such form factors. At present, one must rely on model predictions for the matter densities and test those against proton scattering data.

Proton and neutron ground-state densities have been determined for a wide range of nuclei from Skyrme-Hartree-Fock (SHF) calculations, and extensive comparisons for the charge densities have been made with available data from electron scattering [3]. The good agreement generally found reflects on the adequacy of the calculated matter densities, which are used as input for the calculation of proton elastic scattering observables in this work. Analyses of proton scattering data from ^{208}Pb using SHF models have been made [4], whereby the neutron skin thickness in ^{208}Pb was determined. One corollary of the latter was the observation that analyses of zero momentum transfer data are not enough to elicit sufficient information on the densities of nuclei. Data taken at finite momentum transfer are also required. For analyses of proton scattering data to have credibility, as tests of the underlying structures assumed for the target nuclei, one must have a model of scattering for which there are no parameters to be fitted to the data being analysed. Only then may one evaluate the models used to specify the nuclear structure without ambiguity.

The matter densities obtained from the assumed structure models (shell, SHF, and SHF with shell-model occupancies) have been used with realistic nucleon-nucleon interactions in a folding model, requiring no *a posteriori* fitting [5], to specify optical potentials for the elastic scattering of protons with energies in the range $25 - 200$ MeV. Those potentials are then used to make predictions for differential cross sections and spin observables for proton scattering, a procedure that has been applied extensively [5]. Comparisons are then made to available proton scattering data. When using that folding model with the SHF densities, those allowed for the recognition of a signature for exotic structures in neutron-rich isotopes in the reaction cross sections [6]. The present work extends that earlier work to consider the effects on the elastic scattering observables.

II.   THE SKYRME-HARTREE-FOCK DENSITY CALCULATIONS

Charge-density distributions and the associated nuclear radii have been calculated with the Hartree-Fock method for comparison with available data from electron scattering [3]. Two forms of the Skyrme interaction have been used for the calculations, the so-called SKX$_{csb}$ [7] and SKM* [8] interactions. The SKX$_{csb}$ Hamiltonian is based on the SKX Hamiltonian [9] with a charge-symmetry-breaking (CSB) interaction, added to account for nuclear displacement energies [7]. The charge densities from SKX and SKX$_{csb}$ are essentially identical, so the SKX$_{csb}$ results will be referred to as "SKX". The SKX and SKM* results for the charge densities are very similar, the main difference being that the interior density is about 5% higher with SKM*, with marginally better overall agreement with experiment for SKM*. Generally good agreement between theory and experiment has been achieved in extensive comparisons of measured nuclear charge-density distributions with calculated values for p-shell, sd-shell, and fp-shell nuclei and some selected magic and semi-magic nuclei up to Pb. The extent of the agreement is further improved by constraining the Hartree-Fock equations to use occupation numbers from large-basis shell model calculations. Somewhat larger deviations are observed for lighter nuclei, which may imply the inadequacy of the mean-field approximation [3]. The good agreement with experiment for electron scattering data is a justification for using the proton and neutron radial wave functions as input for the optical model calculations.

For the purposes of the present study, we have used both the basic SHF (denoted SHF henceforth) densities and those obtained from the SHF constrained by use of the shell model occupation numbers (denoted as SHF-SM). (Those numbers are listed in Table I for the isotopes considered herein.) For the sd-shell, the USD interaction of Wildenthal and Brown [10] as well as the USDB interaction of Brown and Richter [11], in the case of the neutron-rich nuclei, were used. For those nuclei in which the neutrons extend to the fp-shell the $sdpf$-U interaction of Nowacki and Poves [12] was used in the $sdpf$-model space. No spuriosity is admitted into the wave functions as the protons are restricted to be solely within the sd-shell. All calculations of the occupation numbers were done using the NuShell shell-model code [13]. For comparison, we have also used shell model wave functions where indicated for the lighter isotopes, and used a simple packed shell model in which the lowest orbits are filled, with no configuration mixing.

III.   CALCULATION OF PROTON SCATTERING OBSERVABLES

To calculate microscopically the differential cross sections and spin observables for NA scattering, one generally begins with an effective nucleon-nucleon (NN) interaction. That interaction is folded with the ground-state density of the target nucleus to obtain the microscopic optical potential from which the observables are obtained. Herein, we utilise the Melbourne approach, which is described in detail in a review [5]; we give a brief outline to highlight the important aspects of this model below.

To obtain a credible effective NN interaction one usually starts with the g matrices of the free NN interaction. Those g matrices are solutions of the Brueckner-Bethe-Goldstone (BBG) equations for infinite nuclear matter, *viz.*

$$g\left(\mathbf{q}', \mathbf{q}; \mathbf{K}\right) = V\left(\mathbf{q}', \mathbf{q}\right) + \int V\left(\mathbf{q}', \mathbf{k}'\right) \frac{Q\left(\mathbf{k}', \mathbf{K}; k_f\right)}{\left[E\left(\mathbf{k}, \mathbf{K}\right) - E\left(\mathbf{k}', \mathbf{K}\right)\right]} g\left(\mathbf{k}', \mathbf{q}; \mathbf{K}\right) d\mathbf{k}', \qquad (1)$$

TABLE I. Shell-model occupation numbers, as used in the SHF-SM calculations, for the given orbits.

(Nomenclature: $4 = 0d_{5/2}, 5 = 0d_{3/2}, 6 = 1s_{1/2}, 7 = 0f_{7/2}, 8 = 0f_{5/2}, 9 = 1p_{3/2}, 10 = 1p_{1/2}$)

Z	Isotope	Orbits	Proton occupancies	Neutron occupancies
14	^{28}Si	4, 5, 6	$4.623, 0.673, 0.704$	$4.623, 0.673, 0.704$
16	^{32}S	4, 5, 6	$5.421, 1.161, 1.418$	$5.421, 1.161, 1.418$
16	^{34}S	4, 5, 6	$5.607, 0.736, 1.657$	$5.674, 2.484, 1.752$
16	^{36}S	4, 5, 6	$5.869, 0.237, 1.894$	$6.000, 4.000, 2.000$
16	^{38}S	4, 5, 6	$5.766, 0.762, 1.472$	
		7, 8, 9, 10		$1.636, 0.088, 0.242, 0.034$
16	^{40}S	4, 5, 6	$5.727, 1.302, 0.972$	
		7, 8, 9, 10		$3.350, 0.156, 0.443, 0.052$
18	^{36}Ar	4, 5, 6	$5.761, 2.500, 1.740$	$5.761, 2.500, 1.740$
18	^{38}Ar	4, 5, 6	$5.946, 2.109, 1.945$	$6.000, 4.000, 2.000$
18	^{40}Ar	4, 5, 6	$5.920, 2.200, 1.880$	
		7, 8, 9, 10		$1.750, 0.060, 0.160, 0.030$
18	^{44}Ar	4, 5, 6	$5.840, 2.659, 1.491$	
		7, 8, 9, 10		$5.359, 0.193, 0.397, 0.051$
20	^{40}Ca	5, 6, 7, 9	$3.090, 1.800, 0.990, 0.120$	$3.090, 1.800, 0.990, 0.120$
20	^{42}Ca	7, 8, 9, 10		$1.812, 0.058, 0.110, 0.021$
20	^{44}Ca	7, 8, 9, 10		$3.674, 0.126, 0.171, 0.029$
20	^{48}Ca	5, 6, 7, 9	$3.550, 1.630, 0.750, 0.070$	$3.830, 1.960, 7.910, 0.300$

where Q is a Pauli blocking operator, and effects of the mean field are incorporated into the auxiliary potentials entering the energy denominator. The centre-of-mass and Fermi momenta are denoted by K and k_f, respectively.

The g matrices obtained from the BBG equations are mapped to a coordinate-space representation to give an effective g matrix (g_{eff}) which is complex, energy- and density-dependent. When that effective interaction is folded with a reasonable microscopic model structure of the target for the nucleus, one obtains the NA optical potential of the form,

$$U\left(\mathbf{r}, \mathbf{r}'; E\right) = \delta\left(\mathbf{r} - \mathbf{r}'\right) \sum_i n_i \int \varphi_i^*(\mathbf{s}) g_D\left(\mathbf{r}, \mathbf{s}; E\right) \varphi_i(\mathbf{s})\, d\mathbf{s} + \sum_i n_i \varphi_i^*(\mathbf{r}) g_E\left(\mathbf{r}, \mathbf{r}'; E\right) \varphi_i(\mathbf{r}')$$

$$= U_D\left(\mathbf{r}; E\right) \delta\left(\mathbf{r} - \mathbf{r}'\right) + U_E\left(\mathbf{r}, \mathbf{r}'; E\right), \tag{2}$$

where the subscripts D, E denote the (local) direct and (nonlocal) exchange parts of the optical potential, respectively. The sums are taken over the bound state single-particle orbits for which n_i are the associated occupation numbers. We use a variant of the DWBA98 program [14] to calculate the optical potential and observables using SHF single-particle wave functions. The resultant complex, energy-, and density-dependent g-folding optical potential contains central, two-body spin-orbit, and tensor terms. As there are no parameter adjustments to fit to the data being described, all model results are predictions.

TABLE II. Isotopes considered for the elastic scattering of protons. References for the available data are given.

Nuclei	References
^{28}Si	[15], [16]
^{32}S, ^{34}S, ^{36}S, ^{38}S, ^{40}S	[15], [17], [18], [19], [20], [21]
^{36}Ar, ^{38}Ar, ^{40}Ar, ^{42}Ar, ^{44}Ar	[22], [23]
^{40}Ca, ^{42}Ca, ^{44}Ca, ^{46}Ca, ^{48}Ca, ^{50}Ca, ^{52}Ca, ^{54}Ca	[23], [24]
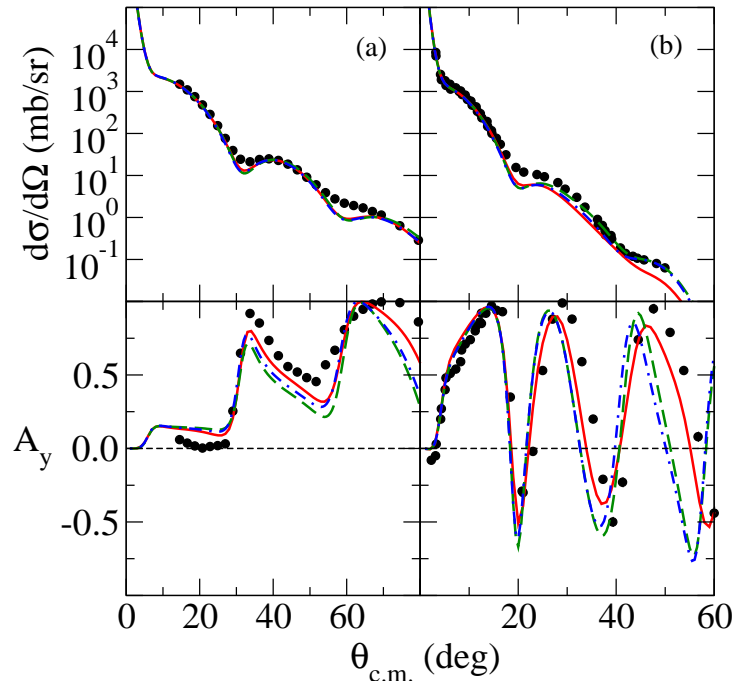
FIG. 1. (Color online.) Differential cross sections and analysing powers for the elastic scattering of 65 [(a)] and 200 MeV [(b)] protons from ^{28}Si. The data are compared to the results of calculations made using the shell, SHF, and SHF-SM models.

IV. COMPARISONS WITH DATA

We present analyses with reference to various isotopes of S, Ar, and Ca, as listed in Table II, together with references to available data as used in these analyses. In the following diagrams, except when explicitly specified, the results of the calculations made using the shell (or packed shell), SHF, and SHF-SM models are denoted by the solid, dashed, and dot-dashed lines, respectively.

Before considering the S, Ar, and Ca isotopes, we consider scattering from ^{28}Si, as there are many data available for this stable nucleus. Of the elastic proton scattering data available, we have chosen to analyse those data taken at 65 MeV [15] and 200 MeV [16], as there have been extensive analyses of data for a range of nuclei at both energies [25], resulting in the effective NA interactions at both energies being well-established. Fig. 1 presents the differential cross sections and analysing powers for the elastic scattering of protons from
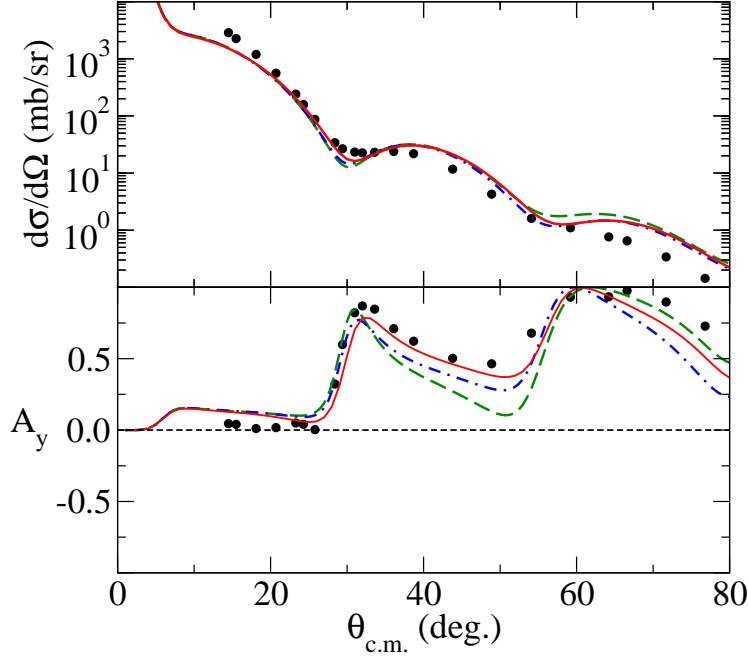
FIG. 2. (Color online.) Differential cross sections and analysing powers for the elastic scattering of 65 MeV protons from ^{32}S. The data are compared to the results of calculations made using the shell, SHF, and SHF-SM models.

^{28}Si, wherein the data are compared to the results of the calculations made using wave functions from the shell, SHF, and the SHF-SM models. The oscillator length for the harmonic oscillator single-particle wave functions used in the shell model calculation was 1.85 fm. For 65 MeV scattering there is very little difference in the predictions for the differential cross sections between the three models used; they do equally well in describing the data. Differences emerge in the analysing power, with the shell model result doing best of all, although all three results describe the shape and magnitudes well. While the three models do well to describe the forward-angle differential cross section at 200 MeV, both SHF models do better in predicting the cross section above 20°. In the results for the analysing power at that energy, the shell-model result deviates significantly from the SHF results above 20° but are in better agreement with the data.

A. The S isotopes

Fig. 2 displays the results of calculations made for the elastic scattering of 65 MeV protons from ^{32}S. Therein, the data [15] are compared to the results obtained from the shell ($b = 1.85$ fm), SHF, and SHF-SM models. All three models give a reasonable representation of the differential cross-section data to 60°, but overestimate the differential cross section at larger angles. The differences between the models are far more noticeable in the analysing power, for which the shell model result gives clearly the best agreement with data. Of the two SHF models, the model with the shell model occupancies defined *a priori* gives the better agreement. This is of note as ^{32}S is mid-shell and the occupancies are expected to play a significant role. We have also considered the elastic scattering of 29.6 MeV protons
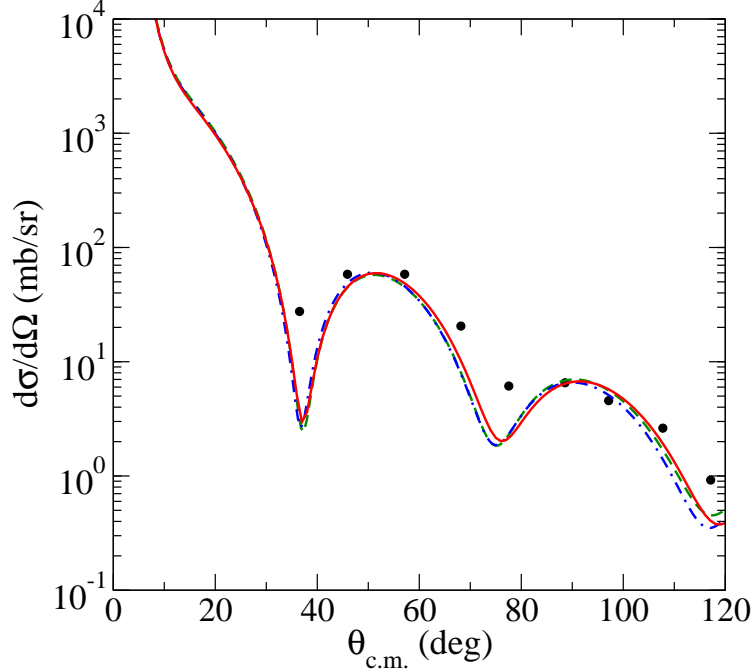
6

FIG. 3. (Color online.) As for Fig. 2 but for 29.6 MeV protons.

from ^{32}S, the results of which are shown in Fig. 3. There is agreement between all the models and reasonable agreement with the data [17]. It is worth noting that the present analysis reproduces the shape and magnitude well, without the need for *ad hoc* renormalisations of potentials or the use of the phenomenological M_n/M_p ratios [21], which has been shown to be problematic [26].

The results of the calculations from the three models for the scattering of 29.8 MeV protons from ^{34}S are compared to the data [18] in Fig. 4. For ^{34}S, there is very little difference between the results obtained using the shell model (the same oscillator length was used as for ^{32}S) or either of the SHF models. All results are in quite reasonable agreement with the available data [18]. This is consistent with the results for the scattering at 29.6 MeV for ^{32}S.

Fig. 5 shows the differential cross section for the elastic scattering of 28 MeV protons from ^{36}S. Therein, the results of the calculations made using the shell ($b = 1.9$ fm), SHF, and SHF-SM models are compared to the data [19]. All models do equally well in describing the data, although the level of agreement between the results and the data above 35° is somewhat poorer. Considering the problems in specifying the microscopic optical potentials below 30 MeV [5], the level of agreement is still reasonable. A previous JLM analysis [21] was able to reproduce the data, but only by renormalising the real and imaginary parts of the potential. Also, in that case, the isovector part of the JLM potential was increased by a factor of 2.0. No such renormalisations were required in the potential for the results in the present work.

The differential cross section for the elastic scattering of 39 MeV protons from ^{38}S is shown in Fig. 6. Therein, the three models ($b = 1.9$ fm for the packed shell model) are compared to the data [20]. All the models do equally well in describing the data up to 30°. All the models underestimate the data in the region of the minimum, up to 40°. The previous JLM model result [21] required a larger renormalisation of the imaginary part of
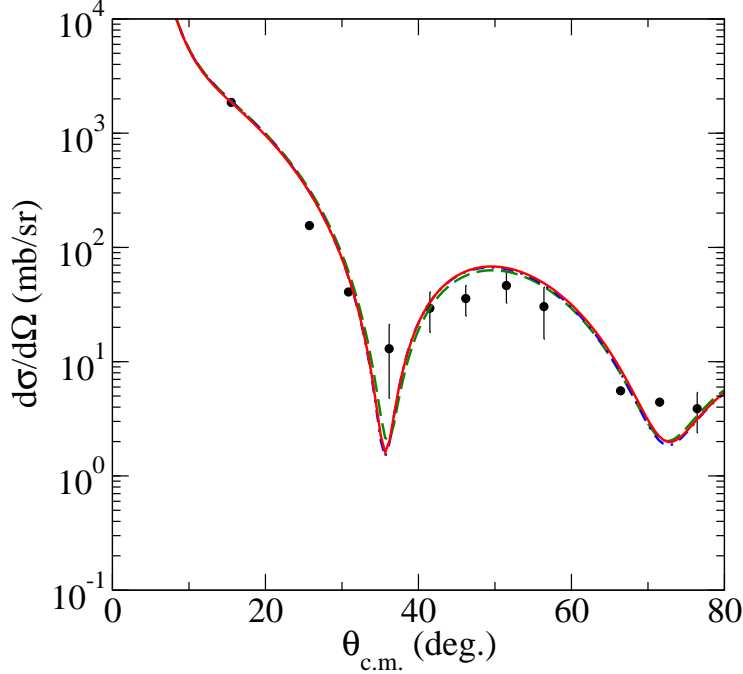
FIG. 4. (Color online.) As for Fig. 2 but for the elastic scattering of 29.8 MeV protons from ^{34}S.

the potential compared to the real part, which was not in keeping with the normalisations that model required for the lighter isotopes.

Fig. 7 shows the differential cross section for 30 MeV elastic scattering of protons from ^{40}S. Therein, the data [21] are compared to the results from the packed shell ($b = 1.9$ fm), SHF, and SHF-SM models. All the results compare equally well with the data, and once more no renormalisations in the potentials were necessary in achieving these results. However, the level of agreement is difficult to gauge given the large error bars in the data.

B.   The Ar isotopes

We now turn our attention to the Ar isotopes, beginning with ^{36}Ar. Fig. 8 shows the comparison of the data to the results of the calculations made using the wave functions from the shell ($b = 1.85$ fm), basic SHF, and SHF-SM models. All model results agree with the data up to 32° quite well. However, beyond that the model results do not reproduce either the shape or the magnitude of the data, although the SHF-SM result does marginally better than the other two. An earlier microscopic (JLM model) analysis [22] required independent renormalisations of the real and imaginary parts of the effective NA interaction of 0.94 and 0.92, respectively, to fit the data. One cannot conclude as to whether the reproduction of the data is due to the underlying description of the nucleus, or the renormalisations of the potential. Also, those data beyond 30° do not define a sharp diffraction minimum, even one that may be smoothed by experimental resolution. Another measurement may be required to explain the anomalies between the models' predictions and to confirm the data.

Fig. 9 presents the results of calculations made for the elastic scattering of 33 and 65 MeV protons from ^{38}Ar using wave functions from the three models, where $b = 1.85$ fm is used for the shell model densities. There is very little difference between the three models.
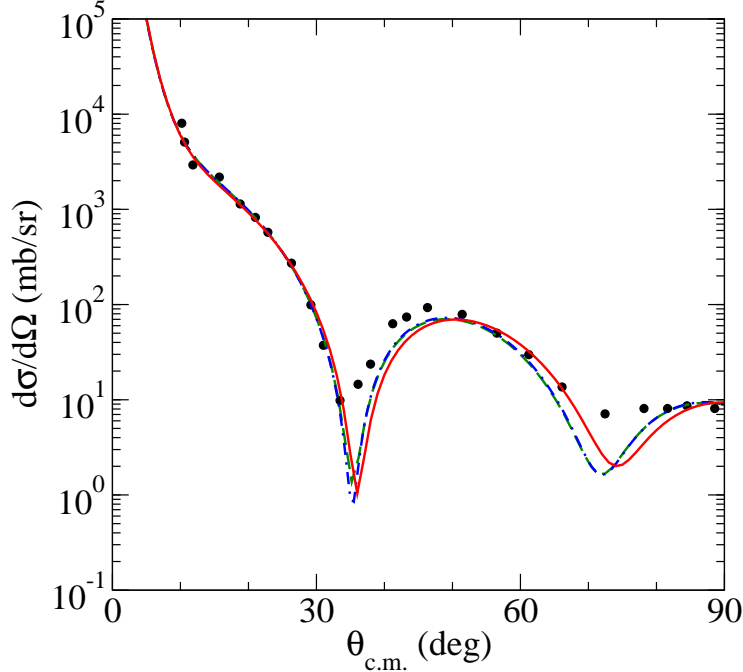
FIG. 5. (Color online.) As for Fig. 2, but for the elastic scattering of 28 MeV protons from ^{36}S.

The differential cross sections and analysing powers for the elastic scattering of 65 MeV protons from ^{40}Ar are displayed in Fig. 10. Therein, the differential cross-section and analysing power data [23] are compared to the results of the calculations made using a simple packed shell model ($b = 1.85$ fm), the SHF, and SHF-SM models. Of the three results, the best agreement with the data comes from using the simple packed model. The differential cross section is well reproduced also by the SHF model, while the SHF-SM model does marginally less well. For the analysing power, all three models explain the data reasonably well, though the best agreement is obtained with the packed shell model.

Fig. 11 shows the differential cross sections for the 33 MeV elastic scattering of protons from ^{42}Ar and ^{44}Ar. Therein, the data [22] are compared to the results of the calculations made using the simple packed ($b = 1.85$ fm and 1.88 fm for ^{42}Ar and ^{44}Ar, respectively), the SHF, and SHF-SM models. For both nuclei, there is no difference between the SHF and SHF-SM results. For ^{36,42,44}Ar, the models all give good results for scattering to $\sim 30°$, and underestimate the cross section at larger angles. While the discrepancy is not as severe, and there is some agreement between the model results and the data at larger angles in magnitude and shape, we note that these data are from the same experiment as that for ^{36}Ar. The JLM analysis presented in the earlier work [22] required the same renormalisations of the real and imaginary parts. There is consistency in those JLM analyses but the question remains as to whether the level of agreement is due to the underlying structure or the renormalisations themselves.

C. The Ca isotopes

The differential cross section and analysing power for the elastic scattering of 65 MeV protons from ^{40}Ca are displayed in Fig. 12. Therein, the data [23] are compared to the
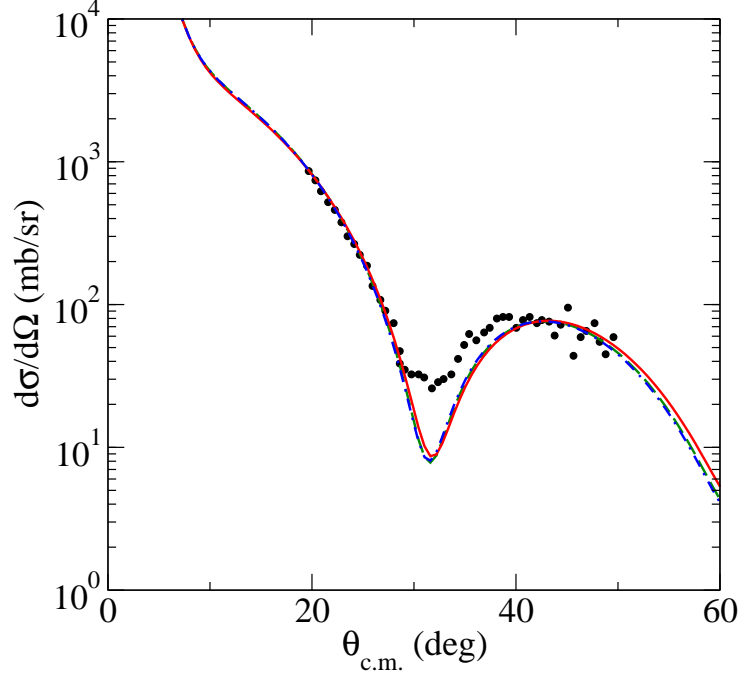
FIG. 6. (Color online.) As for Fig. 2, but for the elastic scattering of 39 MeV protons from ^{38}S. The shell model used in this case is a packed model.

results of calculations made using the packed shell ($b = 1.9$ fm), the SHF, and SHF-SM models. All models do equally well in describing the differential cross-section data to 80°. It is in the analysing power that differences emerge, with the packed shell model providing a better description of the data.

Fig. 13 shows the differential cross section for the elastic scattering of 65 MeV protons from ^{42}Ca. The data [24] for the differential cross section are well described by the shell ($b = 1.9$ fm) and both SHF models, as was the case for scattering from ^{40}Ca. As with ^{40}Ca, the packed shell model does better at describing the analysing power. Note that the results from the SHF models are identical, as the ground-state wave function is largely $(0f_{\frac{7}{2}})^2_\nu$, as indicated by the occupation numbers.

A similar observation may be reached for the comparison of the results of the calculations made from the packed shell ($b = 1.9$ fm) and SHF models with data for the elastic scattering of 65 MeV protons from ^{44}Ca, for which the differential cross section and analysing power are displayed in Fig. 14. Therein, the data [23] are compared to the results of the three model calculations. The results for the differential cross section compare quite well with the data, while the analysing power data are better described by the packed shell model result. As with ^{42}Ca, both SHF models give identical results, as the ground state is predominantly $(0f_{\frac{7}{2}})^4_\nu$.

^{48}Ca provides for an interesting test of the SHF models, as that nucleus is very well described by a filled $0f_{\frac{7}{2}}$ neutron shell. Fig. 15 displays the differential cross section and analysing power for 65 MeV elastic proton scattering from ^{48}Ca. The data [23] are compared to the results of the calculations made using all three models, where the shell model is a closed $0f_{\frac{7}{2}}$ neutron orbit ($b = 1.9$ fm). All three results of the model calculations compare very well with the data. Yet, the SHF and SHF-SM models are almost in complete agreement:
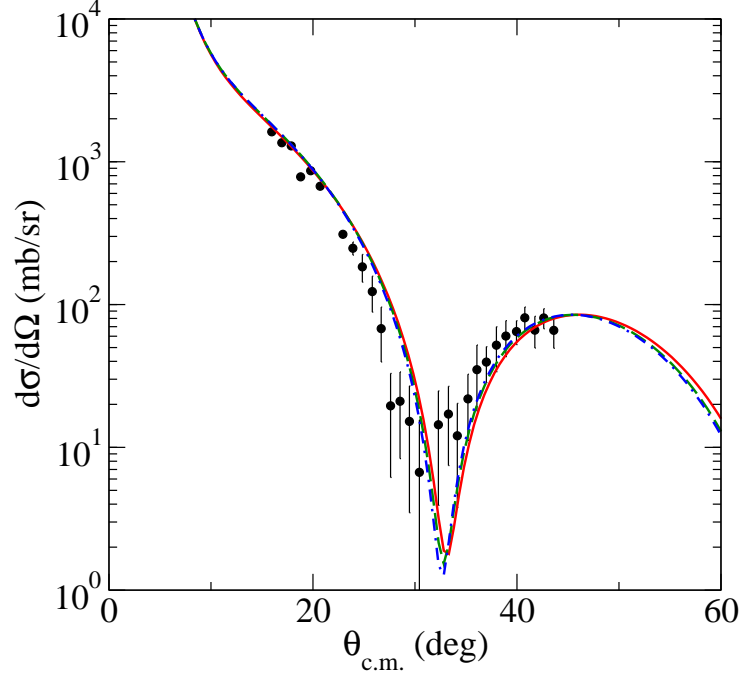
FIG. 7. (Color online.) As for Fig. 6, but for the elastic scattering of 30 MeV protons from ^{40}S.
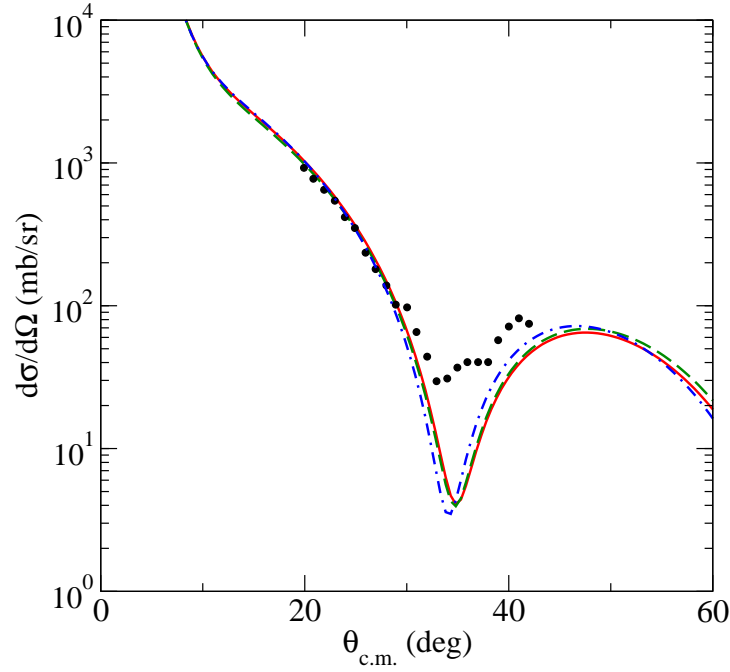

FIG. 8. (Color online.) Differential cross section for the elastic scattering of 33 MeV protons from ^{36}Ar. The data [22] are compared to the results of the calculations made using wave functions obtained from the shell, the SHF, and the SHF-SM models.
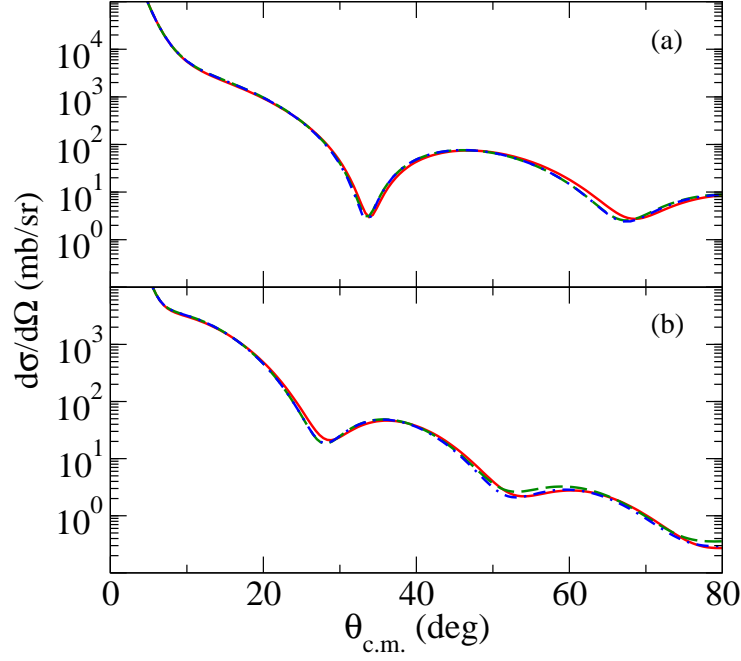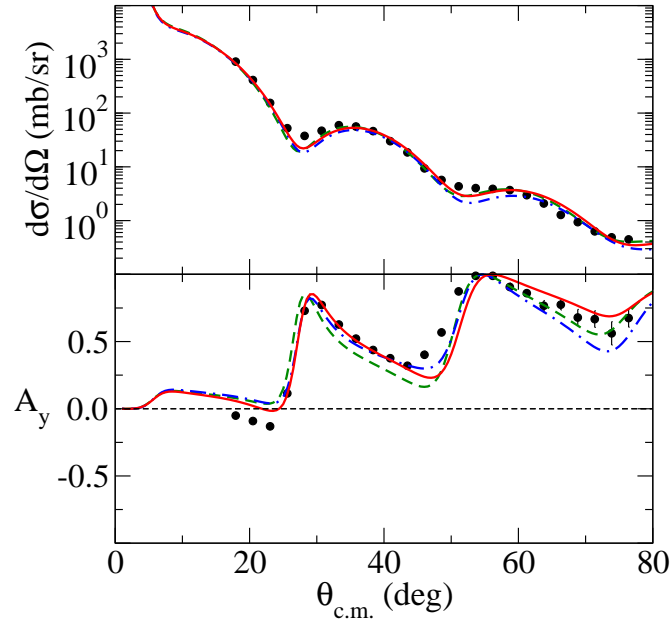
FIG. 9. (Color online.) Comparison of the differential cross sections obtained from calculations made using the shell, SHF, and SHF-SM models for the elastic scattering of 33 MeV (a) and 65 MeV (b) protons from ^{38}Ar.

FIG. 10. (Color online.) Differential cross section and analysing power for the elastic scattering of 65 MeV protons from ^{40}Ar. The data [23] are compared to the calculations made using a packed shell, the SHF, and the SHF-SM models.
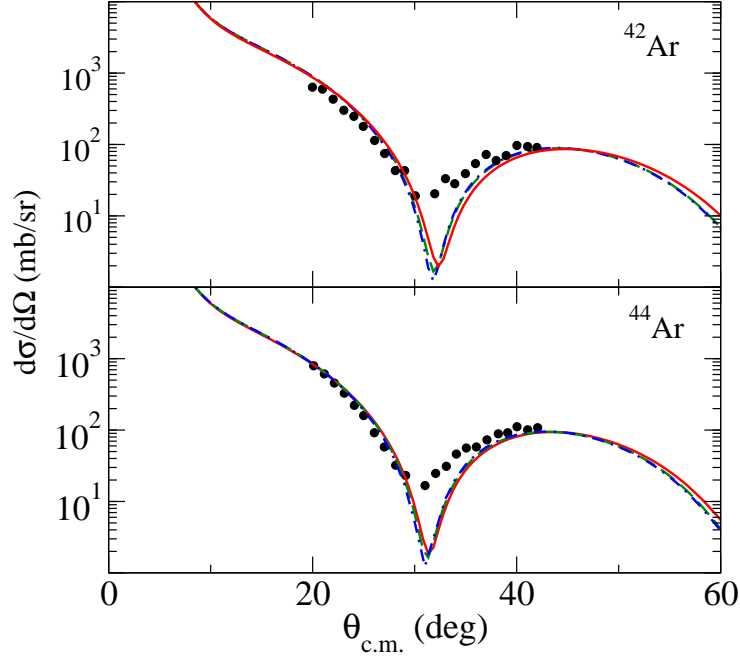
FIG. 11. (Color online.) Differential cross sections for the scattering of 33 MeV protons from ^{42}Ar and ^{44}Ar. The data [22] are compared to the results of the calculations from the packed shell, SHF, and SHF-SM models.
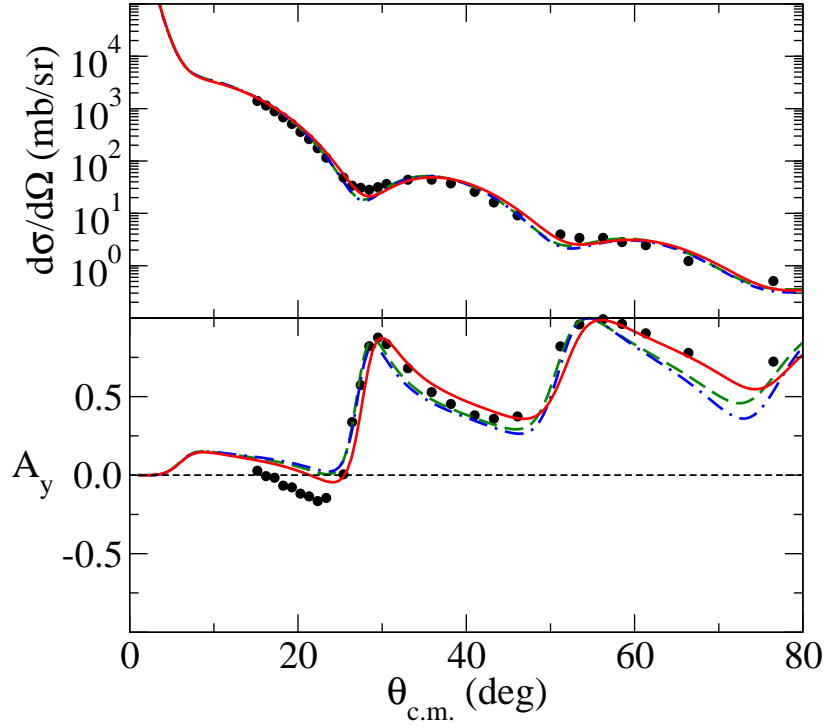

FIG. 12. (Color online.) Differential cross section and analysing power for the elastic scattering of 65 MeV protons from ^{40}Ca. The data [23] are compared to the results of the calculations performed using a packed shell, SHF, and SHF-SM models.
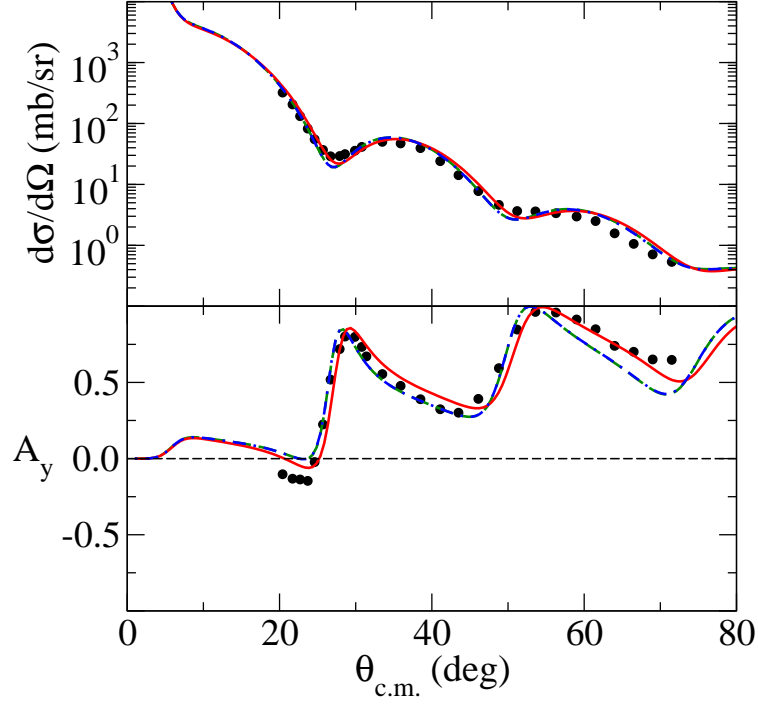
FIG. 13. (Color online.) Differential cross section and analysing power for the elastic scattering of 65 MeV protons from ^{42}Ca. The data [24] are compared to the results of the packed shell model, SHF, and SHF-SM calculations.
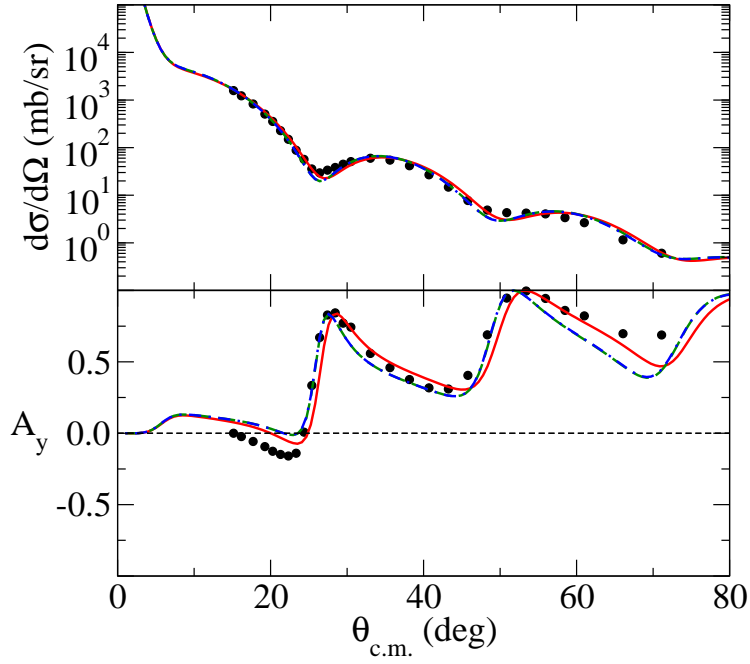

FIG. 14. (Color online.) Differential cross section and analysing power for the elastic scattering of 65 MeV protons from ^{44}Ca. The data [23] are compared to the results of the calculations from the packed shell, SHF, and SHF-SM models.
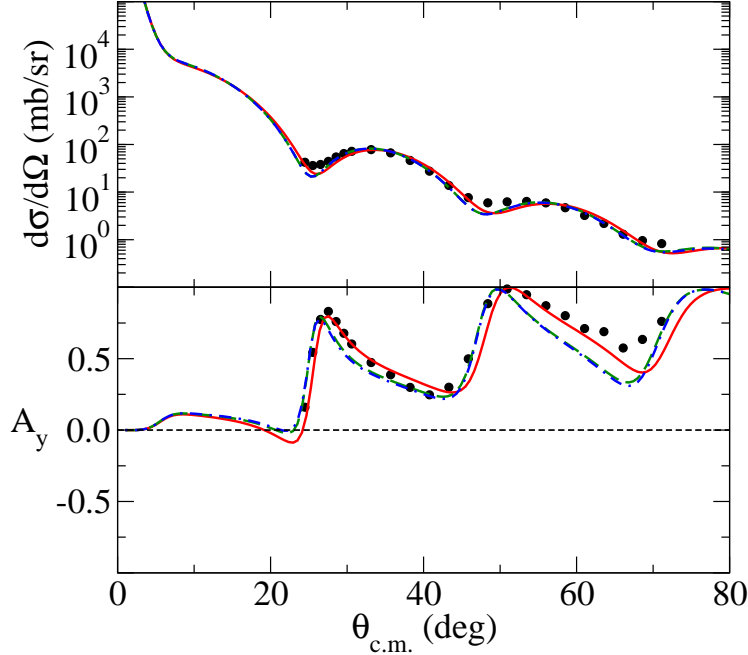
FIG. 15. (Color online.) As for Fig. 12 but for the scattering from ^{48}Ca.

the SHF assumes a closed $0f_{\frac{7}{2}}$ neutron orbit, while the occupancies used in constraining the SHF-SM, listed in Table I, indicate some mixing in ^{48}Ca. The degree of that mixing is small, and that is evident in the nearly identical predictions made between the SHF and SHF-SM models, for both the differential cross section and analysing power.

Fig. 16 displays the differential cross sections for the elastic scattering of 65 MeV protons from all even-even Ca isotopes from ^{40}Ca to ^{54}Ca. Therein, the SHF model was used to obtain the differential cross sections. As shown in the figure, there is a clear mass dependence in the differential cross section, as expected. Whether the cross sections for the heaviest Ca isotopes may be measured remains an academic question as it depends on the availability of suitable Ca beams. It is hoped that such beams will become available, as there is a question of the presence of a magic number either at ^{52}Ca or ^{54}Ca [27]. As the spin-orbit force may change close to the drip line, it has been suggested [27] that the $0f_{\frac{5}{2}}$ orbit falls below the $1p_{\frac{3}{2}}$, in which case ^{52}Ca would no longer be doubly-magic.

V. CONCLUSIONS

We have presented results of calculations of elastic scattering of protons from isotopes of S, Ar, and Ca, using models based on Skyrme-Hartree-Fock methods. Two such models were used: one, the standard SHF, while the other constrained the Hartree-Fock iterations by specifying the nucleon occupancies, obtained from the shell model, *a priori*. For comparison, the shell model was also used to calculate the scattering observables.

Comparisons of results from calculations of proton elastic scattering from ^{28}Si indicated that using densities obtained from either the SHF models was as good, if not better, than using those from the shell model. Of the two SHF models, the SHF-SM model was found to be slightly better.
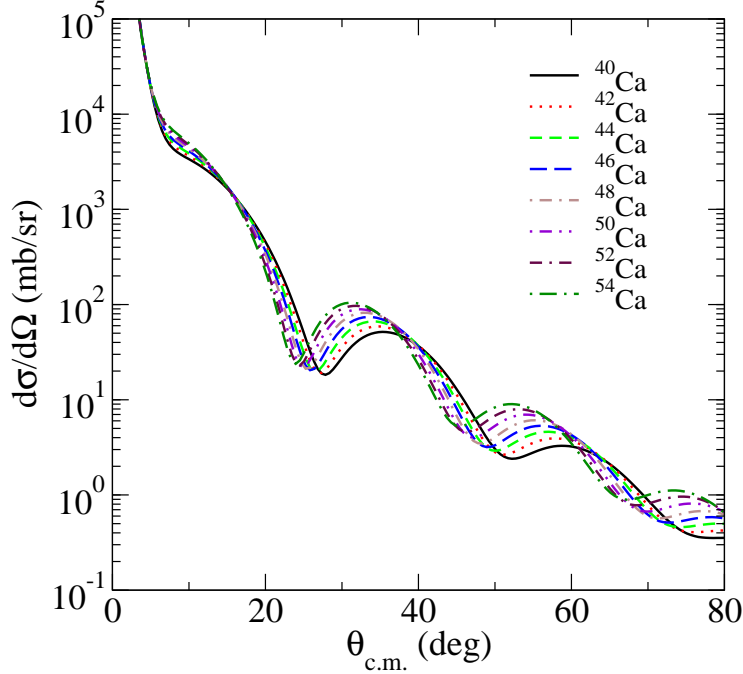
15

FIG. 16. (Color online.) Differential cross sections for the elastic scattering of 65 MeV protons from all even-even Ca isotopes from ^{40}Ca to ^{54}Ca. The SHF model was used to obtain the cross sections.

That the SHF-SM model gives a better description of the nuclear density was evident for ^{32}S since the differential cross section and analysing power were better described using that model structure. However, for the heavier isotopes of sulfur, that was not the case. Using either model for the structure, equivalent descriptions of the elastic scattering data were obtained. The shell model constraint on the Hartree-Fock procedure did not improve the level of agreement. It is of note that the descriptions of the elastic scattering worsened for large angles in these cases; serious renormalisations were required of the JLM potentials to obtain fits to the data. As the specification of the Melbourne potential does not allow for such renormalisations, we hope that more data may be collected to confirm the data used herein. The same conclusions were reached for the Ar isotopes, for which more data are also needed.

The Ca isotopes provided a sensitive control on the specification of the SHF densities, as ^{48}Ca is very well described by a filled $0f_{\frac{7}{2}}$ neutron shell. In that case, one expects the SHF and SHF-SM results to be equal. This was shown to be so in the analyses of the differential cross-section and analysing-power data for the elastic scattering. Also, we considered the mass dependence on the scattering from ^{40}Ca to ^{54}Ca and found that dependence to be smooth. As there is interest in the descriptions of the structures of ^{52}Ca and ^{54}Ca, we hope that scattering data will be measured in the future when beams of those two exotic nuclei become available.

Together with the reaction cross section, measurements of the differential cross sections will elicit much information on the structures of these neutron-rich nuclei. With the increase in the number of radioactive beam facilities it is hoped that not only will there be data taken for new nuclei, but also of those already available to provide valuable confirmation of previous experiments.

ACKNOWLEDGMENTS

[1] T. Suda and M. Wakasugi, Prog. Part. Nucl. Phys. **55**, 417 (2005); T. Suda *et al.*, Phys. Rev. Lett. **102**, 102501 (2009).

[2] *Technical Proposal for the Design, Construction, Commissioning, and Operation of the ELISe setup*, spokesperson Haik Simon, GSI Internal Report, Dec. 2005.

[3] W. A. Richter and B. A. Brown, Phys. Rev. C **67**, 034317 (2003).

[4] S. Karataglidis, K. Amos, B. A. Brown, and P. K. Deb, Phys. Rev. C **65**, 044306 (2002).

[5] K. Amos, P. J. Dortmans, H. V. von Geramb, S. Karataglidis, and J. Raynal, Adv. in Nucl. Phys. **25**, 275 (2000).

[6] K. Amos, W. A. Richter, S. Karataglidis, and B. A. Brown, Phys. Rev. Lett. **96**, 032503 (2006).

[7] B. A. Brown, W. A. Richter, and R. Lindsay, Phys. Lett. **B483**, 49 (2000).

[8] J. Bartel, P. Quentin, M. Brack, C. Guet, and M. B. Hakansson, Nucl. Phys. **A386**, 79 (1982).

[9] B. A. Brown, Phys. Rev. C **58**, 220 (1998).

[10] B. A. Brown and B. H. Wildenthal, Ann. Rev. Nucl. Part. Sci. **36**, 29 (1988).

[11] B. A. Brown and W. A. Richter, Phys. Rev. C **74**, 034315 (2006).

[12] F. Nowacki and A. Poves, Phys. Rev. C **79**, 014310 (2009).

[13] NuShell Programme. http://www.nscl.msu.edu/∼brown/resources/resources.html.

[14] J. Raynal, "computer program dwba98, nea 1209/05," (1998).

[15] S. Kato *et al.*, Phys. Rev. C **31**, 1616 (1985).

[16] K. H. Hicks *et al.*, Phys. Rev. C **38**, 229 (1988); J. Lui *et al.*, iUCF Scientific and Technical Report, 1992, p. 11.

[17] R. de Leo, G. D'Erasmo, E. M. Fiore, G. Guarino, and A. Pantaleo, Nuovo Cimento A **59**, 101 (1980).

[18] R. Alarcon, J. Rapaport, R. T. Kouzes, W. H. Moore, and B. A. Brown, Phys. Rev. C **31**, 697 (1985).

[19] A. Hogenbirk, H. P. Blok, M. G. E. Brand, A. G. M. van Hees, J. F. A. van Hienen, and F. A. Jansen, Nucl. Phys. **A516**, 205 (1990).

[20] J. H. Kelley *et al.*, Phys. Rev. C **56**, R1206 (1997).

[21] F. Maréchal *et al.*, Phys. Rev. C **60**, 034615 (1999).

[22] H. Scheit *et al.*, Phys. Rev. C **63**, 014604 (2000).

[23] H. Sakaguchi, M. Nakamura, K. Hatanaka, A. Goto, T. Noro, F. Ohtani, H. Sakamoto, H. Ogawa, and S. Kobayashi, Phys. Rev. C **26**, 944 (1982).

[24] T. Noro, H. Sakaguchi, M. Nakamara, K. Hatanaka, F. Ohtani, H. Sakamoto, and S. Kobayashi, Nucl. Phys. **A366**, 189 (1981).

[25] P. J. Dortmans, K. Amos, and S. Karataglidis, J. Phys. G **23**, 183 (1997); P. J. Dortmans, K. Amos, S. Karataglidis, and J. Raynal, Phys. Rev. C **58**, 2249 (1998).

[26] K. Amos and S. Karataglidis, arXiv:1007.0365, submitted to Phys. Rev. C.

[27] M. Honma, T. Otsuka, B. A. Brown, and T. Mizusaki, Phys. Rev. C **65**, 061301(R) (2002).